Chemistry & Biology
Resource

Brain Region Mapping Using Global Metabolomics

Julijana Ivanisevic,[1] Adrian A. Epstein,[2] Michael E. Kurczy,[1] Paul H. Benton,[1] Winnie Uritboonthai,[1] Howard S. Fox,[2] Michael D. Boska,[3] Howard E. Gendelman,[2,*] and Gary Siuzdak[1,*]
[1]Scripps Center for Metabolomics and Mass Spectrometry, The Scripps Research Institute, 10550 North Torrey Pines Road, La Jolla, CA 92037, USA
[2]Department of Pharmacology and Experimental Neuroscience, College of Medicine, University of Nebraska Medical Center, Omaha, NE 68198, USA
[3]Department of Radiology, College of Medicine, University of Nebraska Medical Center, Omaha, NE 68198, USA
*Correspondence: hegendel@unmc.edu (H.E.G.), siuzdak@scripps.edu (G.S.)
http://dx.doi.org/10.1016/j.chembiol.2014.09.016

SUMMARY

Historically, studies of brain metabolism have been based on targeted analyses of a limited number of metabolites. Here we present an untargeted mass spectrometry-based metabolomic strategy that has successfully uncovered differences in a broad array of metabolites across anatomical regions of the mouse brain. The NSG immunodeficient mouse model was chosen because of its ability to undergo humanization leading to numerous applications in oncology and infectious disease research. Metabolic phenotyping by hydrophilic interaction liquid chromatography and nanostructure imaging mass spectrometry revealed both water-soluble and lipid metabolite patterns across brain regions. Neurochemical differences in metabolic phenotypes were mainly defined by various phospholipids and several intriguing metabolites including carnosine, cholesterol sulfate, lipoamino acids, uric acid, and sialic acid, whose physiological roles in brain metabolism are poorly understood. This study helps define regional homeostasis for the normal mouse brain to give context to the reaction to pathological events.

INTRODUCTION

Metabolomics entails the elucidation of the biochemical processes engaged at the systems level (e.g., cell, tissue, or organismal) via the measurement of the end products of cell activity. The subdiscipline of central nervous system (CNS) metabolomics has recently emerged as a part of basic and applied clinical investigations into degenerative, infectious, cancerous, and inflammatory disorders (Dumas and Davidovic, 2013; Mandal et al., 2012; Nicholson et al., 2012). The role of metabolomics in brain disease rests in measuring and deciphering the spectrum of small molecules that affect neurophysiologic (e.g., neurotransmitters, signaling lipids, and osmolytes) and cell signaling (e.g., regulators of cytokines and of oxidative stress, intermediary and energy currency metabolites) life processes (Piomelli et al., 2007). The creation of a detailed map of the human neural network (known as the *connectome*) (Sporns, 2011) and its metabolic bridge will help to build a knowledge base to unravel complex brain functions. For example, assessment of intraneural and interneural communications and complex interactions among brain regions and subregions will ultimately define how metabolites mediate neural function. This is of vital importance since brain metabolism goes beyond neurotransmission and the variations in energy metabolism underlie normal homeostasis and the complex pathobiology in a broad range of CNS disorders (Cai et al., 2012; Davidovic et al., 2011; Dumas and Davidovic, 2013; Holmes et al., 2006; Prabakaran et al., 2004)

Although the use of metabolomics for studies of neural function, in health and disease, is gaining critical attention, this field still faces real challenges related, in part, to the intrinsic inaccessibility of the metabolome (Griffin and Salek, 2007; Rae, 2014). While biofluid metabolite profiling of cerebrospinal fluid (CSF), plasma, and urine have been applied, their limitations are well recognized. One notable obstacle to the use of biofluids to reflect nervous system pathobiology is the blood-brain barrier (BBB) that serves to limit the passage of metabolites from the periphery. Thus, the degree to which biofluids (specifically plasma and urine) mirror brain health or disease, in particular, is contested (Domange et al., 2011; Griffin and Salek, 2007). Indeed, to unequivocally gain access to the brain metabolome, the tissue must be considered. Human brain tissue, while being the most relevant to study, is difficult to procure, especially in the case of control samples. Such studies are further complicated by postmortem delays that may affect metabolite degradation. Therefore, studies in relevant animal models of human health and disease are crucial. Animal models, including transgenic and humanized mice, can mirror human disease events (Gorantla et al., 2012) and enable the "true" metabolomics expressed in the phenotype to assess complex neural processes (Domange et al., 2011).

Among the analytical techniques used in metabolomics, high resolution proton NMR (^{1}H-NMR) and liquid-chromatography-mass spectrometry (LC/MS) are widely applied for biofluid profiling, whereas high resolution magic angle spinning NMR and magnetic resonance spectroscopy (MRS) are used to analyze brain tissue (Blüml et al., 2013; Domange et al., 2011). Among molecular imaging assays, MRI and positron emission tomography have enabled in vivo anatomical and functional studies (Rae, 2014). The ex vivo imaging of brain tissue can be performed by several mass spectrometry-based techniques (Hanrieder et al., 2013): MALDI (Cerruti et al., 2012; Fournier et al., 2011; Murphy et al., 2009), secondary ion mass spectrometry (Hanrieder et al., 2014; Sjövall et al., 2004), and

nanostructure initiator mass spectrometry (NIMS) (Lee et al., 2012; Patti et al., 2010). These techniques are mainly used for the analysis of functional brain peptides and lipids.

A majority of brain metabolism studies employ a targeted analysis of a small set of known, well defined metabolites (Bathena et al., 2012; Ivanisevic et al., 2013; Yanes et al., 2011). For example, ^{1}H-NMR has been used to uncover specific highly abundant metabolites (N-acetyl-aspartate, myo-inositol, glutamate, glutamine, creatine, choline, and GABA). Such studies have proven to be a key for the characterization of neurochemical and metabolic profiles relevant to brain health (Davidovic et al., 2011; Liu et al., 2013; Pears et al., 2005; Prabakaran et al., 2004; Tkác et al., 2004). Granting high reproducibility, the MR technologies are restricted by their low sensitivity, which hinders comprehensive pathologic assessments. Compared with NMR, mass spectrometry has the advantage of being a highly sensitive approach that can capture the variation of thousands of metabolites, including those present at relatively low concentrations (as low as picomolar) (Ivanisevic et al., 2013; Yanes et al., 2011). Surprisingly, metabolic profiling using LC/MS, which is the most versatile technique in metabolomics, has rarely been applied to brain tissue (Graham et al., 2013; Inoue et al., 2013). While targeted approaches are focused on analyses of a defined, limited number of metabolites, untargeted assays profile thousands of metabolite features without an a priori hypothesis (Patti et al., 2012b, 2012c). Such holistic analyses can uncover unanticipated roles of specific metabolites and the associated biochemical pathways. To achieve this goal, we have performed global metabolite profiling across anatomical regions of the brain, using high-throughput, high-resolution mass spectrometry. The NOD/SCID/IL2R$\gamma c^{-/-}$ (NSG) mouse was chosen for its abilities to support humanization and its rapid evolving utilities in developing novel therapeutic strategies for infectious and cancerous diseases (McDermott et al., 2010; Rongvaux et al., 2014). Focused beam microwave irradiation (FBMI) was applied to deliver a high power pulse to induce instant euthanasia, simultaneously halting brain enzyme activities (Epstein et al., 2013). Effectiveness of FBMI was validated in each animal using noninvasive postmortem ^{1}H-MRS of brain tissue. A complex brain metabolome was successfully recovered by hydrophilic interaction liquid chromatography-electrospray ionization-mass spectrometry (HILIC-ESI-MS). The acquired signatures of each brain region enabled the definition of differential metabolite patterns or metabotypes. The diversity of metabolite patterns across the brain and its relation to region-specific function was further investigated through multigroup comparison by the analysis of most discriminative metabolites. Nanostructure imaging mass spectrometry (NIMS) of brain tissue allowed for complementary and subregional spatial distribution of specific metabolites. The information about region-specific metabolite enrichments reported here provides a link between the anatomical and functional differences among brain regions.

RESULTS AND DISCUSSION

Global Metabolomics of Brain Anatomy Using LC/MS and NIMS Profiling

Studies of brain metabolism at the regional level are surprisingly scarce and when performed generally use targeted approaches to interrogate a small subset of metabolites whose physiological roles are well described. The current untargeted LC/MS approach, in concert with the power of matrix-free NIMS, has been developed for simultaneous measurement of large numbers of diverse metabolites with a broad range of functional properties. Liquid chromatography coupled to mass spectrometry is considered as the most comprehensive and versatile technique of choice for global metabolite profiling efforts (Patti et al., 2012c). To integrate LC/MS profiling and NIMS, one brain hemisphere was dissected and each region was separately extracted for untargeted LC/MS analyses (mice specimens = 5), while the other (intact) hemisphere was used for NIMS analyses (Figure 1). The application of an amino-based column for LC/MS profiling and the amino-based NIMS initiator used for imaging has further facilitated this combined approach for the screening of small polar central carbon metabolites. In this way NIMS has enabled the acquisition of complementary information about the local anatomical distribution of specific ions of interest.

The comprehensive, semiquantitative HILIC-ESI-MS profiling was applied in negative ionization mode to maximize

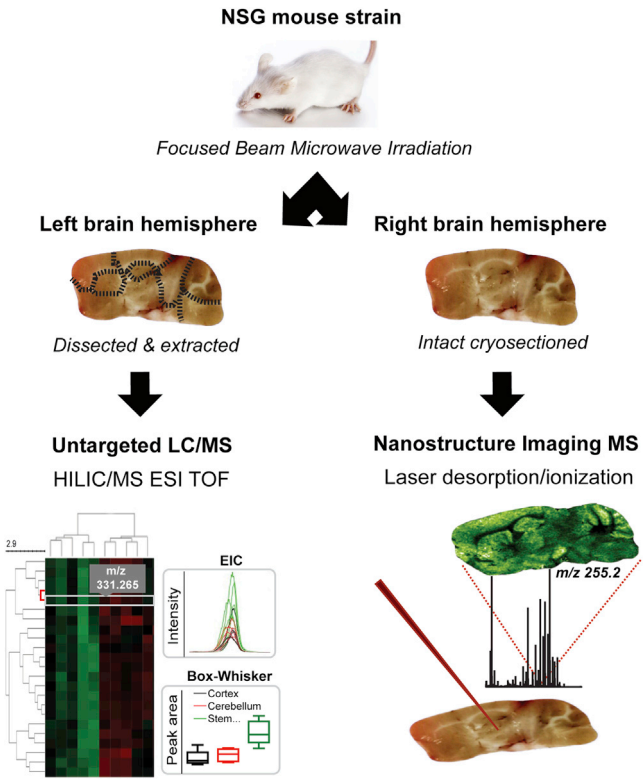

Figure 1. Global Metabolomic Approach for Regional Mapping of Brain Tissue

This workflow integrates two complementary technologies, untargeted LC/MS profiling using hydrophilic interaction chromatography (HILIC) coupled to electrospray ionization (ESI) mass spectrometry and nanostructure imaging mass spectrometry (NIMS). Following the heat fixation (FBMI), the left brain hemisphere was dissected and each brain region was extracted separately for untargeted LC/MS profiling (mice specimens = 5). The intact right brain hemisphere was imaged by laser desorption-ionization mass spectrometry to create maps of spatial distribution of metabolites of interest across the brain and within each subregion.

metabolome coverages (Ivanisevic et al., 2013). The differential metabolite profiles (*metabotypes*) were acquired for the frontal cortex, dorsal cortex, ventral cortex, striatum, hippocampus, thalamus-midbrain, brain stem, and cerebellum. The analytical strategy of hydrophilic interaction enabled the detection of 15,835 lipid and water-soluble metabolite features across all brain regions, including the highly abundant, well-characterized brain metabolites (Fei et al., 2014) (e.g., glutamate, taurine, N-acetylaspartate [NAA], N-Acetylaspartylglutamic acid [NAAG]; Figure S3 available online). Each of these metabolite features corresponds to a detected ion with a unique mass-to-charge ratio and a unique retention time (Patti et al., 2012a; Yanes et al., 2011). It should be noted that metabolites can be defined by several metabolite features matching isotope, adduct, and in-source fragment peaks. In parallel to major classes of abundant phospholipids (e.g., phosphatidylcholines [PC], phosphatidylethanolamines [PE], phosphatidylserines [PS], phosphatidylinositols [PI], and phoshoglycerols [PG]) hydrophilic profiling of brain regions permitted detection of central carbon metabolites, nutrients, and metabolic byproducts of cellular metabolism. These included nucleotides, amino, nonamino organic acids, and specific neuropeptides (Figures S1–S3). Although LC/MS has often been used for biofluid profiling to identify the metabolite biomarkers of specific brain dysfunction, this highly sensitive technique has rarely been applied to brain tissue profiling (Graham et al., 2013). It is likely that even when brain tissue is available, from biopsies or in postmortem conditions, key metabolites may be lost due to rapid enzyme degradation. Rapid fixation is critical to avoid hypoxia-related changes and metabolite degradation in brain tissue. While flash freezing in liquid nitrogen, as commonly used in metabolomics, may be suitable for peripheral organs (e.g., lung, muscle, kidney, liver, and pancreas), even the short delay between brain isolation and fixation results in metabolic alterations under hypoxemic conditions (Griffin and Salek, 2007). Additionally, metabolites are degraded at different rates, which further complicate analysis (de Graaf et al., 2009; Detour et al., 2011). In particular, glucose and energy-linked phosphates are prone to degradation within seconds of mammalian death (Lowry et al., 1964). Key to detecting and measuring these metabolites was the use of FBMI, which precludes rapid metabolite degradation in the brain (Epstein et al., 2013; O'Callaghan and Sriram, 2004). When FBMI is applied to live anesthetized mice instant euthanasia ensues, quenching cellular metabolism including enzyme activities (Epstein et al., 2013). The efficiency of FBMI fixation was evaluated using ^{1}H-MRS. Specifically, NAA and lactic acid levels were measured and compared with levels measured in living anesthetized mice. Samples with reduced levels of NAA and increased lactic acid were discarded. It has been demonstrated that NAA is synthesized in the mitochondria of neurons and thus hypoxia may reduce NAA by reduction in mitochondrial metabolism (Bates et al., 1996). To avoid further changes in metabolite levels and dissipation of local concentration gradients of other metabolites, the brains ($n = 5$) were dissected and frozen within 30 min of FBMI. It should also be noted that the results presented here are representative of mice in a sleep state as metabolic pathways are differentially regulated and specific areas of the brain may be less active during anesthesia. To this point, FBMI could be adapted to quench brain metabolism during an awake state and/or during a specific task (e.g., sensory stimulation) in order to avoid the potential effects of anesthesia on brain metabolism.

Fixation methods, such as funnel freezing or the application of microwaves on an intact live brain coupled to ^{1}H-MRS validation, as used in this report, ensure the efficient quenching of metabolism (Detour et al., 2011). When metabolism quenching is performed correctly, the advantage of brain tissue over biofluid profiling is significant as limited passage of metabolites by BBB, and differences between the brain parenchyma and CSF, present major pitfalls for the use of biomarkers from biofluid analysis. The analysis of brain tissue samples provides unique information about localized metabolic activity.

Metabolite Patterns across Anatomical Brain Regions

The knowledgebase for regional distribution of brain metabolites is contradictory (Minati et al., 2010) and limited to a small set of molecules that can be profiled in vivo by proton magnetic resonance spectroscopy (Pouwels and Frahm, 1998). The results of these studies, although not global in their scope, have already demonstrated variation in metabolite concentrations across different brain regions. In this report multigroup analysis of global LC/MS profiles was used to characterize the diversity and variation of a broad range of metabolites across anatomical brain regions. Multigroup comparison is an extension of the traditional two-group experimental design (control versus disease) that permits broad comparisons of three or more sample classes (Gowda et al., 2014). Untargeted LC/MS profiling in hydrophilic interaction mode followed by multigroup comparison enabled the identification of a large number of differentially expressed metabolite features across eight profiled brain regions. A total of 561 significant differences ($p \leq 0.01$) were observed in the lipid and water-soluble brain metabolome, as shown on the cloud plot (Figure 2). For example, the variation pattern of glycerophosphoserine (22:6/22:6) revealed significantly higher content in the brain stem and cerebellum in comparison with cortex and other brain regions (Figure 2B). Among hydrophilic metabolites, NAAG, a highly abundant neurotransmitter, was present in significantly higher levels in thalamus-midbrain, brain stem, and cerebellum compared with the cortex, striatum, and hippocampus (Figure 2B). These results were in accordance with the concentrations determined by quantitative localized proton MRS, which specified that NAAG increased caudally and exhibited higher concentrations in white matter than in gray matter (Pouwels and Frahm, 1998). Multigroup analysis also confirmed that NAA (in contrast to NAAG) was distributed homogeneously throughout the brain (Figure S3).

Variation patterns of 60 significantly fluctuating metabolites ($p \leq 0.01$, $q \leq 0.001$) were used to cluster the brain regions (Figure 3; Figures S1–S3). Hierarchical clustering analysis (HCA) revealed two distinct groups. One comprised the midbrain, cerebellum, and brain stem and the other comprised the cortex, hippocampus and striatum. The samples within the first cluster formed three separate subgroups matching specific brain regions: cerebellum, brain stem (pons-medulla), and thalamus-midbrain. The samples within the second major cluster were sorted randomly into smaller subgroups, not relevant to specific brain regions. Thalamus-midbrain, cerebellum, and brain stem were characterized by specific, differential metabolite profiles in comparison with the cortex, striatum, and hippocampus,

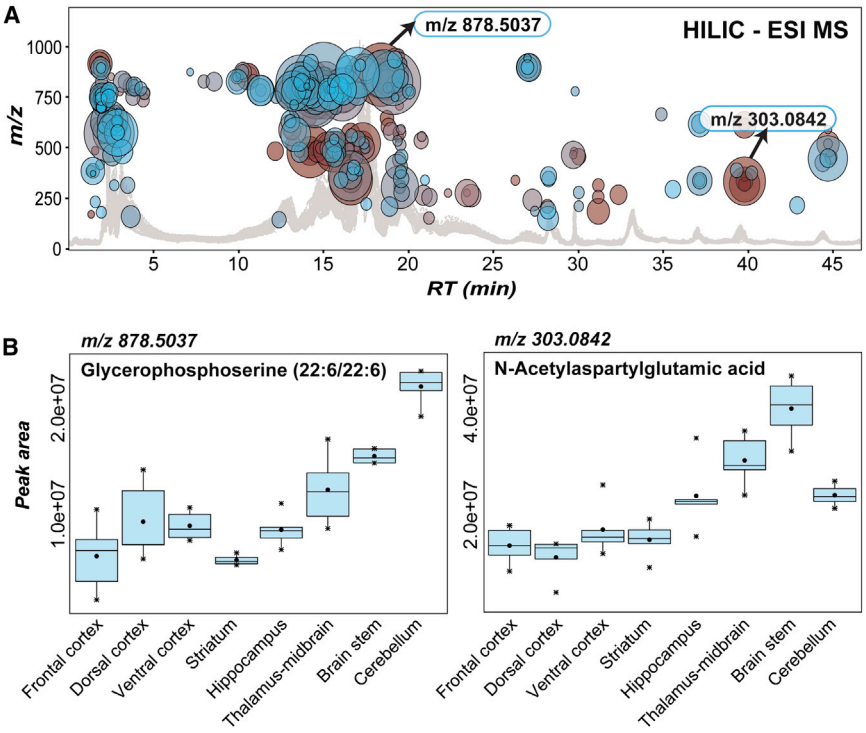

Figure 2. Representation of Global Metabolomic Data with a Focus on Significant Differences in Metabolite Patterns across Brain Regions

(A) Multigroup cloud plot showing differentially expressed metabolite features (bubbles) across different regions of brain (level of significance: $p \leq 0.01$, intensity > 20,000 ion counts). Metabolite features are projected depending on their m/z ratio and retention time. The color of the bubble indicates the level of significance (p value), with darker color (in red tones) representing lower p values. A total ion chromatogram is shown in the background.

(B) Variation patterns of two characteristic lipid and water-soluble brain metabolites across eight different regions of brain. Metabolites were identified on the basis of MS/MS data provided in Figure S5 (NAAG) and in Table S2 (PS 22:6/22:6). ANOVA was used to calculate the statistical significance for n = 5 in each group. Box and whisker plots display the full range of variation (whiskers: median with minimum – maximum; boxes: interquartile range).

which demonstrated higher profile similarities (Figure 3). In general, the orthogonal partial least square discriminant analysis (OPLS-DA) model, using all aligned metabolite features across brain regions (>15,000), supported the HCA classification (Figure 4). Overlapping metabolite patterns in the forebrain that includes cortex, hippocampus, and striatum could support neural connections and hence common metabolic activities (Cenquizca and Swanson, 2007).

Predominant differences among defined regional clusters in the brain were characterized by specific patterns of lipids and their derivatives. In addition to different types of phospholipids (PEs, PCs, PGs, PSs, and PIs), the cholesterol sulfate, two lipoamino acids (N-docosanoyl taurine and N-palmitoyl serine), and phosphoethanolamine were identified among the discriminatory metabolites driving the brain region classification (Figure 3). Cholesterol sulfate displayed a particular variation pattern, characterized by significantly higher levels in the cerebellum as compared with all other brain regions (Figure S1). N-docosanoyl taurine and N-palmitoyl serine demonstrated a similar variation profile with the highest content in thalamus-midbrain and brain stem (Figure S2), while phosphoethanolamine displayed the opposite pattern with the lowest levels in thalamus-midbrain, brain stem, and cerebellum (Figure S1). Beyond specific lipid metabolites, carnosine, and two carboxylic acids, sialic (N-acetylneuraminic acid) and uric acid also contributed to the definition of differential metabolic phenotypes across brain (Figure S1). The highest levels of both carnosine and uric acid were detected in the frontal cortex. The sialic acid pattern showed significantly lower levels in the hindbrain (cerebellum and brain stem).

Taking into consideration the variation patterns of identified lipid and central carbon metabolites, the observed classification of brain regions is likely influenced by a combination of several different factors, including the prevalent neural cell types, white matter tracts (visualized using NIMS imaging vide infra), neurotransmitter profile, and blood vasculature. The gray-to-white matter ratio across specific regions may explain the variation pattern of different lipid metabolites. For instance, as shown by the heatmap (Figure 3), some phospholipids exhibited pronounced regional variability with increasing or decreasing levels depending on the caudally decreasing gradient in gray matter. However, a number of specific glycerophosphoserines displayed significant contrasting levels between frontal and caudal brain regions (Figures 2 and 3), where they may serve as a metabolic reservoir for free serine and regulate serine-dependent neurotransmission (Kopp et al., 2010). Another intriguing finding related to lipid metabolite patterns was a significant high level of cholesterol sulfate in cerebellum when compared with other brain regions. Sulfonation of cholesterol is ubiquitous in cell membranes throughout the body, activating cholesterol for cell adhesion and osmoprotection (Strott and Higashi, 2003). Cholesterol sulfate may regulate the synthesis of cholesterol, which is vital for nerve signal transduction and synaptogenesis, but in excess leads to neurodegeneration (Vance, 2012). However, the specific role of cholesterol sulfate associated to cerebellum function remains to be elucidated.

Furthermore, the evaluation of metabolite patterns across brain regions uncovered high levels of free radical scavengers in the frontal cortex. This includes, notably, uric acid and carnosine, which are known to be antioxidants and neuroprotective agents (Fang et al., 2013; Bae et al., 2013). This regional specificity may be linked to surveillance responses, which serve to reduce oxidative stress and protect against oxidative damage. Uric acid was found at lower levels in patients with cognitive impairment (e.g., Alzheimer's disease, Parkinson's disease, vascular-linked dementia) when compared with aged individuals who enjoy normal mental, motor, and behavioral functions

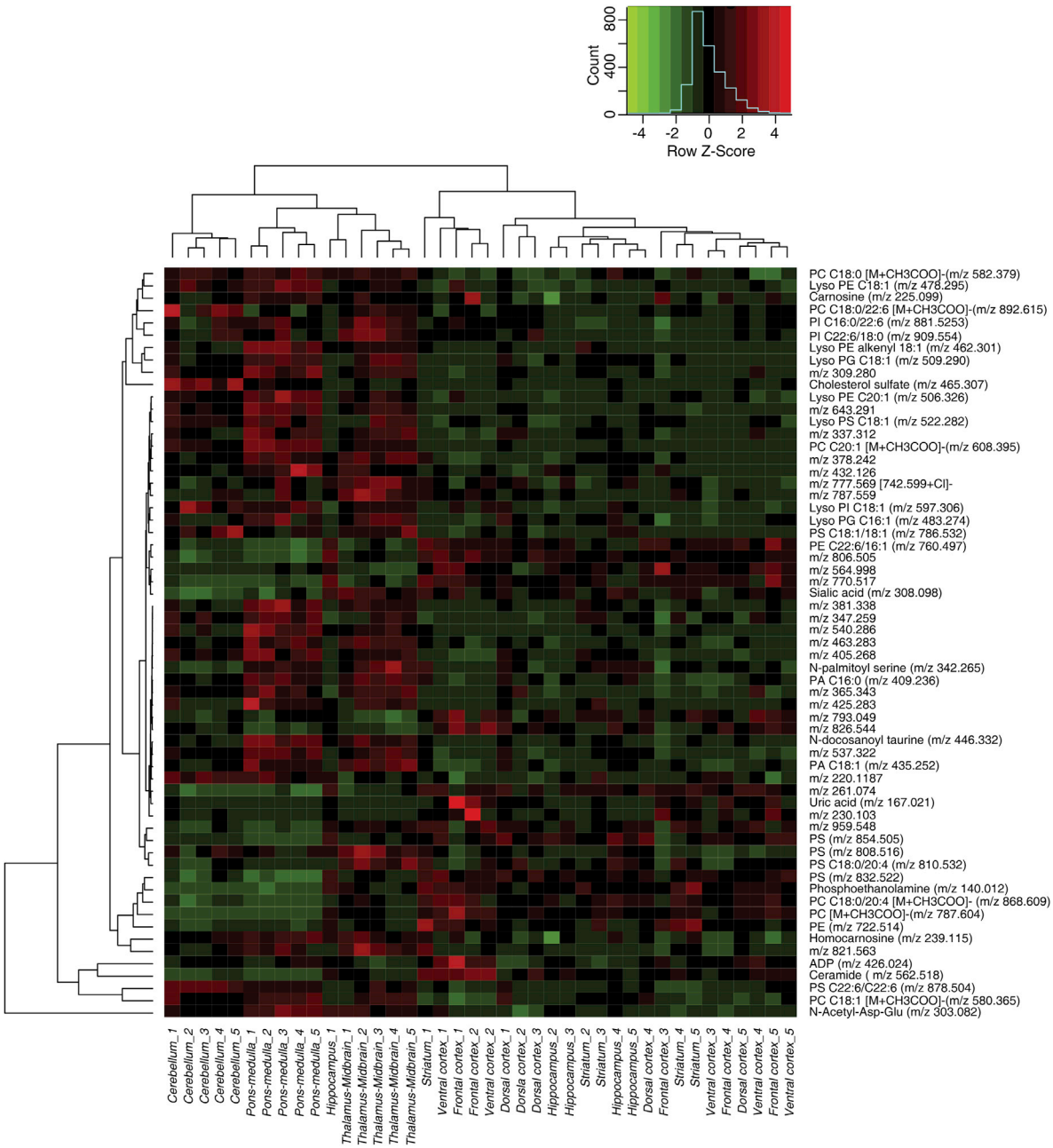

Figure 3. Heatmap and Associated Dendograms Representing the Hierarchically Clustered Samples Based on the Similarity of Metabolite Patterns

Discriminating metabolites (ANOVA $p \leq 0.01$, $q \leq 0.001$, Intensity > 20,000) are shown on the right side. Isotopes, adducts, in-source fragments, and multiply charged features were filtered out. MS/MS data for identified metabolites are provided in Figures S4 and S5. MS/MS patterns for putative identifications of phospholipids are given in Tables S2 and S3. Variation patterns of identified metabolites (with the exception of phospholipids) are presented by box and whisker plots in Figures S1 and S2.

(Gong et al., 2012; Kim et al., 2006). Comparable to uric acid, carnosine is a potent antioxidant that scavenges reactive oxygen species and unsaturated aldehydes leading to reduced oxidative, nitrosative, and glycemic stress (Bellia et al., 2011). Like uric acid, carnosine levels are reduced in Alzheimer's disease, suggesting that carnosine deficiency affects cognitive function (Fonteh et al., 2007). Frontal cortical areas have a complex role in cognitive function and the high content of uric acid and carnosine as homeostatic metabolites may be associated with the need for internal control by the brain in preventing oxidative damage.

Global metabolite profiling provided insights into the unanticipated roles of characteristic metabolites associated with intermediary and energy metabolism as well as membrane

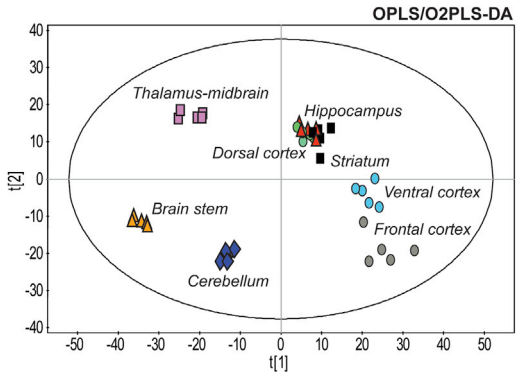

Figure 4. Supervised Pattern Recognition OPLS-DA Model for Metabolomic Profiles of Brain Regions

OPLS scores plot of HILIC-ESI-MS profiles (aligned by XCMS) shows discrimination among specific regions on the first and second component. The model brings out the specific variation of the metabolite composition according to the brain region (five biological replicates per region). Good separation was achieved for three different regions: midbrain, brain stem, and cerebellum. All aligned metabolite features (15,835) were used to create the model, and a total of five orthogonal components were calculated for cross-validation (R2Y(cum) = 0.68, Q2Y(cum) = 0.35).

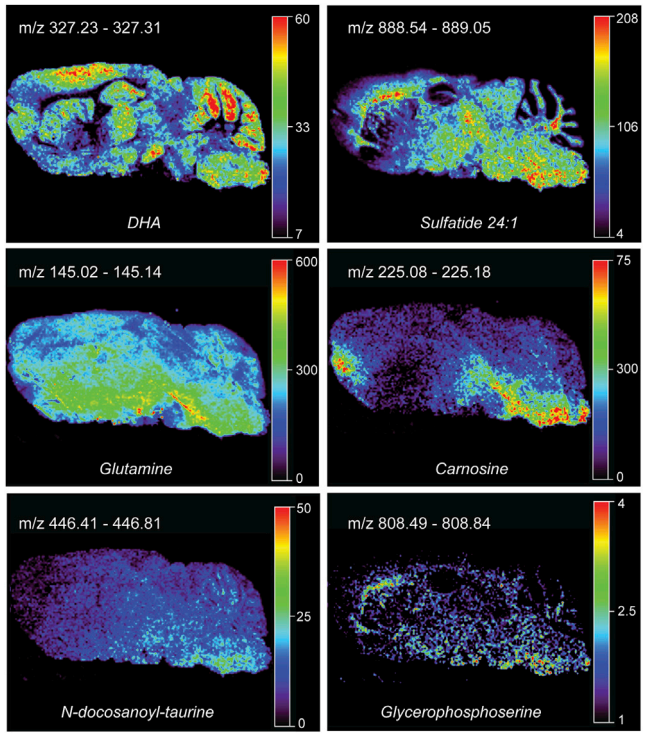

Figure 5. Laser Desorption-Ionization MS Images or Maps of Ions of Interest

Extracted maps from the low mass part of total ion spectra (<500 Da) show the spatial distribution of docosahexaenoic acid (DHA), glutamine, carnosine, and docosanoyl taurine. Extracted maps from the higher mass part of total ion spectra (>800 Da) show the spatial distribution of sulfatide and phosphatidylserine. Images were acquired from a 2 μm thin brain section that was mounted on etched silicon chip, coated with PFUA initiator, prior to imaging in negative ionization mode. Ions of interest were identified using the MS/MS data acquired by LC/MS profiling (Figures S3 and S4; Table S3).

metabolism and neurotransmission. The potential biological connotation of neurochemical changes can be further explored through biochemical assays and/or isotope-labeled tracking experiments to elucidate the active metabolic pathways and functionally better characterize brain regions (Vaishnavi et al., 2010).

NIMS imaging was employed to provide subregional chemical information to aid in the interpretation of global metabolite profiling results. Matrix-free NIMS strategy was introduced based on using pulsed-laser desorption and ionization with a silicon nanostructured surface (Wei et al., 1999). Matrix-free application represents the main advantage over MALDI where the use of organic matrices can present interference when attempting to detect small molecules (less than 500 Da) (Greving et al., 2011). Moreover, laser desorption from the nanostructure surfaces results in efficient energy transfer, low background chemical noise, and the nondestructive release of analyte ions into the gas phase. Detecting these ions as a function of position yields a spatially resolved chemical map of the surface. Nanostructure imaging mass spectrometry of sagittal brain sections provided insights into the spatial distribution of specific metabolites within the profiled anatomical regions. The application of an amino-based initiator to the surface of etched silicon chips facilitated the desorption and ionization and imaging of broader range of negatively charged metabolites (Figure 5). The extracted maps of two specific ions matching docosahexaenoic acid (DHA) and C24:1 sulfatide reflect gray and white matter patterns (Figure 5). DHA is abundant in the gray matter as a developmentally vital component of neuronal membranes and synapses (Salem et al., 2001). Moreover, DHA metabolism is an active process of neuronal membrane functions in the gray matter as seen with radiolabeled DHA uptake and retention rates measured in human brain imaging studies (Umhau et al., 2009). Interestingly, even though these metabolites are differentially distributed throughout the brain they do not contribute to the regional clustering observed using LC/MS analysis because of an averaging effect that is implicit when homogenizing a heterogeneous brain region. The high lateral resolution is additive to the global metabolomics approach in that it provides subregional context, showing the heterogeneity of each region, which is obscured by the gross analysis of the whole.

SIGNIFICANCE

The metabolome is an essential component of brain function. However, its complete characterization poses substantive challenges and as such is limited to a targeted set of highly abundant small molecules investigated through magnetic resonance technology. In order to gain comprehensive insight into the metabolic processes that mediate neural function, we have developed an untargeted mass spectrometry-based approach that permits relative quantification of a broad range of lipid and water-soluble metabolites. The approach combines HILIC/MS and NIMS technology to assess divergent anatomical brain regions including the cortex, striatum, hippocampus, thalamus-midbrain, stem, and cerebellum. Focused microwave beam fixation was performed to limit profile changes related to postmortem delay.

A multigroup comparison of metabolite profiles revealed significant differentially expressed metabolites that were used to hierarchically cluster brain regions. Various phospholipids and several intriguing metabolites, including carnosine, uric and sialic acid, cholesterol sulfate, and lipoamino acids were identified among the most discriminating metabolites. Significant differences in metabolite patterns were observed between the cluster comprising the caudal regions (midbrain, stem, and cerebellum) and the cluster comprising the forebrain regions (cortex, striatum, and hippocampus). The former were each highlighted by specific metabolomic signatures, while the latter displayed similar metabolite patterns. Greater similarity in metabolite patterns could represent a higher level of interaction between brain regions. Brain mapping of the metabolites by NIMS provided complementary information about the metabolite distribution within the brain regions. Overall, the untargeted profiling of brain tissue combined with nanostructure imaging mass spectrometry can encompass a broad range of interacting metabolites with varying chemical and physical properties and thus provide new insights into the complexities of neural function. Additionally, the understanding of regional metabolic differences in the normal brain is essential for understanding the altered pathways in pathological states.

EXPERIMENTAL PROCEDURES

Tissue Preparation

NOD/SCID/IL2R$\gamma c^{-/-}$ (NSG) mouse model is described in the Supplemental Information. Mice were anesthetized with 1%–2% isoflurane in oxygen then aligned in a water-jacketed holder for microwave irradiation in a Muromachi Microwave Fixation System (10 kW model). Irradiation time was 800 ms at 4.9 kW (Epstein et al., 2013). Single voxel localized spectra were acquired postmortem at the midbrain to ensure metabolite level stabilization using point resolved spectroscopy. Spectra were acquired with a repetition time of 4 s, echo time of 50 ms, and 128 averages, using birdcage coil transmit and receive on a 7 Tesla/16 cm Bruker Pharmascan (Karlsure, Germany) MRI/MRS system. Single-scan, localized, unsuppressed water signals were acquired as a reference for metabolite normalization. Brains with abnormal NAA or lactate concentrations were eliminated from further analysis. Five specimens were selected for further brain dissection and analysis. All specimens were from the same genetic strain, males, and of similar ages. The animal studies performed, in support of this research, were approved by the University of Nebraska Medical Center Institutional Animal Care and Use Committee and by established values of the NIH for the ethical care and use of animals.

After spectroscopic validation of FBMI, brains were isolated and initially split into hemispheres, with the left hemisphere reserved for cryosectioning and the right hemisphere dissected into subregions. Subregional dissection followed anatomical boundaries to separate hemi-brains into cerebellum, brain stem (pons and medulla), cerebral cortex, hippocampus, striatum, and midbrain (midbrain and thalamus). Cortex was further divided into frontal, dorsal (somatosensory through visual areas) and ventral (piriform through perirhinal areas) sections. Following dissection, all tissues were flash frozen in liquid nitrogen and stored at −80°C.

Metabolome Extraction

Brain tissue subregions were extracted using a MeOH:H_2O (4:1, v/v) solvent mixture. An adjusted volume of 1 ml of cold solvent was added per 10 mg tissue, probe sonicated for 5 s, and incubated in liquid nitrogen for 1 min. The samples were then allowed to thaw at room temperature and then probe sonicated for another 5 s. To precipitate proteins, the samples were incubated for 1 hr at −20°C, followed by 15 min centrifugation at 13,000 rpm and 4°C. The resulting supernatant was removed and evaporated to dryness in a vacuum concentrator. The pellet was reconstituted in water and protein concentrations were measured using Pierce BCA Protein Assay Kit (Thermo Scientific) as a reference for metabolite reconstitution. The dry extracts were then reconstituted in ACN:H_2O (1:1, v/v) normalized by the sample's protein level, sonicated for 10 min, and centrifuged 15 min at 13,000 rpm and 4°C to remove insoluble debris. The supernatants were transferred to high-performance liquid chromatography vials and stored at −80°C prior to LC/MS analysis.

HILIC/MS Analysis

Tissue extracts (8 brain regions × 5 biological replicates) were analyzed on a 6550 iFunnel QTOF mass spectrometer (Agilent Technologies) interfaced with HPLC 1200 system (Agilent Technologies). Samples were analyzed using a Luna Aminopropyl, 3 μm, 150 × 1.0 mm I.D. HILIC column (Phenomenex). The mobile phase was composed of A = 20 mM ammonium acetate and 40 mM ammonium hydroxide in 95% water and B = 95% acetonitrile (Ivanisevic et al., 2013). The linear gradient elution from 100% B (0–5 min) to 100% A (50–55 min) was applied (A = 95% H_2O, B = 95% ACN, with appropriate additives). A 10 min postrun was applied for HILIC to ensure the column reequilibration and maintain the reproducibility. The flow rate was 50 μl/min, and the sample injection volume was 5 μl. ESI source conditions were set as follows: dry gas temperature 200°C and flow 11 l/min, fragmentor 380 V, sheath gas temperature 300°C and flow 9 l/min, nozzle voltage 500 V, and capillary voltage −2,500 V in ESI negative mode. The instrument was set to acquire over the m/z range 50–1,000, with the MS acquisition rate of 2 spectra/s. For the MS/MS of selected precursors, the default isolation width was set as narrow (~1.3 m/z), with a MS acquisition rate at 2 spectra/s and MS/MS acquisition at 3 spectra/s. MS/MS data were acquired at the collision energy of 20 V and of 40 V.

NIMS

Information about preparation of NIMS surfaces (chips) is provided in the Supplemental Information. Brain hemispheres were frozen in optimum cutting temperature medium (OCT; Sakura Finetek) for cryo-sectioning. Frozen OCT-embedded brain hemispheres were sliced along the sagittal plane into 2 μm sections with a cryostat (Leica Microsystems) and placed on the NIMS chip and immediately dried in a desiccated, room-temperature vacuum chamber. Adjacent brain sections were collected and placed on glass tissue fixation slides for immunofluorescence microscopy and hematoxylin and eosin staining. Thaw-mounted tissue slices were directly imaged using an AB SCIEX TOF/TOF 5800 mass spectrometer (Applied Biosystems), equipped with a Nd:YAG laser at 355 nm, without any sample preparation. Data were acquired at 50 μm spatial resolution in negative ionization mode across the entire brain tissue. Typically, 200 laser shots were collected per spectrum. Propafenone and bradykinin fragments 2–9 were used to calibrate the instrument in the low-mass range. Images were acquired using MS Imaging Tool software with a typical resolution of 50 × 50 μm^2. Data analysis and image reconstruction were performed using BioMap software. Metabolite identifications were deduced from mass value (within 50 ppm accuracy), METLIN matches, and MS/MS data obtained by LC/MS/MS analysis.

Data Analysis

Raw LC/MS data were converted to mzXML files using ProteoWizard MS Convert version 3.0.4146 (Chambers et al., 2012). The mzXML files were uploaded to XCMS Online web platform for data processing (https://xcmsonline.scripps.edu) (Nikolskiy, et al., 2013; Patti et al., 2012a; Smith et al., 2006; Tautenhahn et al., 2012) including peak detection, retention time correction, profile alignment, and isotope annotation. Data were processed as a multigroup design experiment, and the parameter settings were as follows: centWave for feature detection (Δ m/z = 15 ppm, minimum peak width = 10 s, and maximum peak width = 120 s); obiwarp settings for retention time correction (profStep = 1); and parameters for chromatogram alignment, including mzwid = 0.015, minfrac = 0.5, and bw = 5. The relative quantification of metabolite features was based on extracted ion chromatogram (EIC) areas. One-way ANOVA and post hoc Tukey test was used to test the variation pattern of metabolite features across different brain regions (Table S1). The results output, including EICs, and multigroup cloud plot were exported directly from XCMS Online. Metabolite identification was based on accurate mass (within 10 ppm) and MS/MS data. MS/MS data validated via matching against

standards are provided in the Supplemental Information (Figures S4 and S5). Otherwise, the MS/MS fragmentation patterns are provided in Tables S2 and S3.

A heatmap was produced using R version 3.01 and the gplots library. A selection of features whose expression varied significantly across different brain regions ($p < 0.01$, $q < 0.001$, Intensity > 20,000 ion counts) were used to create the heatmap. After filtering out the isotopes, adducts, multiple charged species, and in-source fragments, only the corresponding deprotonated monoisotopic features were used for visualization. A z-transformation was performed on all features to scale the data. Hierarchical clustering analysis (HCA) of metabolite patterns was performed using the Euclidean distance matrix and the complete linkage method.

The orthogonal projection to a latent structure-discriminant analysis (O2-PLS-DA) model was made using SIMCA P+ 12.0 (Umetrics). All aligned metabolite features were used for the analysis. The predictive variance, Q2, was computed by testing on one-seventh of the data. Data were scaled using univariate scaling because this showed the best predictive model. The model was autofitted to find the optimal number of components.

ACCESSION NUMBERS

The ID accession number for the raw metabolomics data reported in this paper is 1017901, and the multigroup brain region comparison overview is available at XCMS Online Public Shares site https://xcmsonline.scripps.edu/jobs.php?action=listpublicshares under the specified ID number and publication name.

SUPPLEMENTAL INFORMATION

Supplemental Information includes Supplemental Experimental Procedures, five figures, and three tables and can be found with this article online at http://dx.doi.org/10.1016/j.chembiol.2014.09.016.

AUTHOR CONTRIBUTIONS

J.I., A.A.E., H.E.G., M.D.B., and G.S. designed the research; A.A.E. and M.D.B. prepared the animals and performed brain region dissection and extraction; J.I. and M.E.K. performed LC/MS/MS and NIMS experiments; J.I. and P.H.B. analyzed the data; and J.I., M.E.K., A.A.E., H.E.G., and G.S. wrote the paper.

ACKNOWLEDGMENTS

We gratefully acknowledge financial support from NIH grants P01 DA026146-02 (G.S.), P01 DA028555, R01 NS36126, P01 NS31492, 2R01 NS034239, P01 MH64570, P01 NS43985, R01 AG043540 (H.E.G.), and P30 MH062261 (G.S., H.S.F., M.D.B., and H.E.G.), and from the Nebraska Research Initiative (M.D.B.), and by the University of Nebraska Foundation, which includes individual donations from Dr. Carol Swarts and Frances and Louie Blumkin and the Vice Chancellor's office of the University of Nebraska Medical Center (H.E.G.). The Center for Translational Mouse Models at the University of Nebraska Medical Center supplied the NSG immunodeficient mice for studies.

Received: July 7, 2014
Revised: September 5, 2014
Accepted: September 18, 2014
Published: November 6, 2014

REFERENCES

Bae, O.N., Serfozo, K., Baek, S.H., Lee, K.Y., Dorrance, A., Rumbeiha, W., Fitzgerald, S.D., Farooq, M.U., Naravelta, B., Bhatt, A., and Majid, A. (2013). Safety and efficacy evaluation of carnosine, an endogenous neuroprotective agent for ischemic stroke. Stroke *44*, 205–212.

Bates, T.E., Strangward, M., Keelan, J., Davey, G.P., Munro, P.M.G., and Clark, J.B. (1996). Inhibition of N-acetylaspartate production: implications for 1H MRS studies in vivo. Neuroreport *7*, 1397–1400.

Bathena, S.P., Huang, J., Epstein, A.A., Gendelman, H.E., Boska, M.D., and Alnouti, Y. (2012). Rapid and reliable quantitation of amino acids and myo-inositol in mouse brain by high performance liquid chromatography and tandem mass spectrometry. J. Chromatogr. B Analyt. Technol. Biomed. Life Sci. *893–894*, 15–20.

Bellia, F., Vecchio, G., Cuzzocrea, S., Calabrese, V., and Rizzarelli, E. (2011). Neuroprotective features of carnosine in oxidative driven diseases. Mol. Aspects Med. *32*, 258–266.

Blüml, S., Wisnowski, J.L., Nelson, M.D., Jr., Paquette, L., Gilles, F.H., Kinney, H.C., and Panigrahy, A. (2013). Metabolic maturation of the human brain from birth through adolescence: insights from in vivo magnetic resonance spectroscopy. Cereb. Cortex *23*, 2944–2955.

Cai, H.L., Li, H.D., Yan, X.Z., Sun, B., Zhang, Q., Yan, M., Zhang, W.Y., Jiang, P., Zhu, R.H., Liu, Y.P., et al. (2012). Metabolomic analysis of biochemical changes in the plasma and urine of first-episode neuroleptic-naïve schizophrenia patients after treatment with risperidone. J. Proteome Res. *11*, 4338–4350.

Cenquizca, L.A., and Swanson, L.W. (2007). Spatial organization of direct hippocampal field CA1 axonal projections to the rest of the cerebral cortex. Brain Res. Brain Res. Rev. *56*, 1–26.

Cerruti, C.D., Benabdellah, F., Laprévote, O., Touboul, D., and Brunelle, A. (2012). MALDI imaging and structural analysis of rat brain lipid negative ions with 9-aminoacridine matrix. Anal. Chem. *84*, 2164–2171.

Chambers, M.C., Maclean, B., Burke, R., Amodei, D., Ruderman, D.L., Neumann, S., Gatto, L., Fischer, B., Pratt, B., Egertson, J., et al. (2012). A cross-platform toolkit for mass spectrometry and proteomics. Nat. Biotechnol. *30*, 918–920.

Davidovic, L., Navratil, V., Bonaccorso, C.M., Catania, M.V., Bardoni, B., and Dumas, M.E. (2011). A metabolomic and systems biology perspective on the brain of the fragile X syndrome mouse model. Genome Res. *21*, 2190–2202.

de Graaf, R.A., Chowdhury, G.M.I., Brown, P.B., Rothman, D.L., and Behar, K.L. (2009). In situ 3D magnetic resonance metabolic imaging of microwave-irradiated rodent brain: a new tool for metabolomics research. J. Neurochem. *109*, 494–501.

Detour, J., Elbayed, K., Piotto, M., Moussallieh, F.M., Nehlig, A., and Namer, I.J. (2011). Ultrafast in vivo microwave irradiation for enhanced metabolic stability of brain biopsy samples during HRMAS NMR analysis. J. Neurosci. Methods *201*, 89–97.

Domange, C.I., Paris, A., Schroeder, H., and Priymenko, N. (2011). Power of a metabonomic approach to investigate an unknown nervous disease. In Neurodegenerative Diseases—Processes, Prevention, Protection and Monitoring, D.R.C.-C. Chang, ed. (Institute for New Technologies). http://dx.doi.org/10.5772/30963.

Dumas, M.E., and Davidovic, L. (2013). Metabolic phenotyping and systems biology approaches to understanding neurological disorders. F1000Prime Rep. *5*, 5–18.

Epstein, A.A., Narayanasamy, P., Dash, P.K., High, R., Bathena, S.P., Gorantla, S., Poluektova, L.Y., Alnouti, Y., Gendelman, H.E., and Boska, M.D. (2013). Combinatorial assessments of brain tissue metabolomics and histopathology in rodent models of human immunodeficiency virus infection. J. Neuroimmune Pharmacol. *8*, 1224–1238.

Fang, P., Li, X., Luo, J.J., Wang, H., and Yang, X.F. (2013). A double-edged sword: uric acid and neurological disorders. Brain Disord. Ther. *2*, 109.

Fei, F., Bowdish, D.M.E., and McCarry, B.E. (2014). Comprehensive and simultaneous coverage of lipid and polar metabolites for endogenous cellular metabolomics using HILIC-TOF-MS. Anal. Bioanal. Chem. *406*, 3723–3733.

Fonteh, A.N., Harrington, R.J., Tsai, A., Liao, P., and Harrington, M.G. (2007). Free amino acid and dipeptide changes in the body fluids from Alzheimer's disease subjects. Amino Acids *32*, 213–224.

Fournier, I., Mériaux, C., Wisztorski, M., Rakwal, R., and Salzet, M. (2011). MALDI imaging mass spectrometry for investigating the brain. In Sample Preparation in Biological Mass Spectrometry, A.R. Ivanov and A.V. Lazarev, eds. (Dordrecht: Springer), pp. 765–783.

Gong, L., Zhang, Q.L., Zhang, N., Hua, W.Y., Huang, Y.X., Di, P.W., Huang, T., Xu, X.S., Liu, C.F., Hu, L.F., and Luo, W.F. (2012). Neuroprotection by urate on 6-OHDA-lesioned rat model of Parkinson's disease: linking to Akt/GSK3β signaling pathway. J. Neurochem. *123*, 876–885.

Gorantla, S., Poluektova, L., and Gendelman, H.E. (2012). Rodent models for HIV-associated neurocognitive disorders. Trends Neurosci. *35*, 197–208.

Gowda, H., Ivanisevic, J., Johnson, C.H., Kurczy, M.E., Benton, H.P., Rinehart, D., Nguyen, T., Ray, J., Kuehl, J., Arevalo, B., et al. (2014). Interactive XCMS Online: simplifying advanced metabolomic data processing and subsequent statistical analyses. Anal. Chem. *86*, 6931–6939.

Graham, S.F., Chevallier, O.P., Roberts, D., Hölscher, C., Elliott, C.T., and Green, B.D. (2013). Investigation of the human brain metabolome to identify potential markers for early diagnosis and therapeutic targets of Alzheimer's disease. Anal. Chem. *85*, 1803–1811.

Greving, M.P., Patti, G.J., and Siuzdak, G. (2011). Nanostructure-initiator mass spectrometry metabolite analysis and imaging. Anal. Chem. *83*, 2–7.

Griffin, J.L., and Salek, R.M. (2007). Metabolomic applications to neuroscience: more challenges than chances? Expert Rev. Proteomics *4*, 435–437.

Hanrieder, J., Phan, N.T.N., Kurczy, M.E., and Ewing, A.G. (2013). Imaging mass spectrometry in neuroscience. ACS Chem. Neurosci. *4*, 666–679.

Hanrieder, J., Gerber, L., Persson Sandelius, Å., Brittebo, E.B., Ewing, A.G., and Karlsson, O. (2014). High resolution metabolite imaging in the hippocampus following neonatal exposure to the environmental toxin BMAA using ToF-SIMS. ACS Chem. Neurosci. *5*, 568–575.

Holmes, E., Tsang, T.M., Huang, J.T., Leweke, F.M., Koethe, D., Gerth, C.W., Nolden, B.M., Gross, S., Schreiber, D., Nicholson, J.K., and Bahn, S. (2006). Metabolic profiling of CSF: evidence that early intervention may impact on disease progression and outcome in schizophrenia. PLoS Med. *3*, e327.

Inoue, K., Tsutsui, H., Akatsu, H., Hashizume, Y., Matsukawa, N., Yamamoto, T., and Toyo'oka, T. (2013). Metabolic profiling of Alzheimer's disease brains. Sci. Rep. *3*, 2364.

Ivanisevic, J., Zhu, Z.-J., Plate, L., Tautenhahn, R., Chen, S., O'Brien, P.J., Johnson, C.H., Marletta, M.A., Patti, G.J., and Siuzdak, G. (2013). Toward 'omic scale metabolite profiling: a dual separation-mass spectrometry approach for coverage of lipid and central carbon metabolism. Anal. Chem. *85*, 6876–6884.

Kim, T.S., Pae, C.U., Yoon, S.J., Jang, W.Y., Lee, N.J., Kim, J.J., Lee, S.J., Lee, C., Paik, I.H., and Lee, C.U. (2006). Decreased plasma antioxidants in patients with Alzheimer's disease. Int. J. Geriatr. Psychiatry *21*, 344–348.

Kopp, F., Komatsu, T., Nomura, D.K., Trauger, S.A., Thomas, J.R., Siuzdak, G., Simon, G.M., and Cravatt, B.F. (2010). The glycerophospho metabolome and its influence on amino acid homeostasis revealed by brain metabolomics of GDE1(-/-) mice. Chem. Biol. *17*, 831–840.

Lee, Y., Platt, V., Bowen, B., Louie, K., Canaria, C.A., McMurray, C.T., and Northen, T. (2012). Resolving brain regions using nanostructure initiator mass spectrometry imaging of phospholipids. Integr. Biol. (Camb.) *4*, 693–699.

Liu, J., Sheldon, R.A., Segal, M.R., Kelly, M.J.S., Pelton, J.G., Ferriero, D.M., James, T.L., and Litt, L. (2013). 1H nuclear magnetic resonance brain metabolomics in neonatal mice after hypoxia-ischemia distinguished normothermic recovery from mild hypothermia recoveries. Pediatr. Res. *74*, 170–179.

Lowry, O.H., Passonneau, J.V., Hasselberger, F.X., and Schulz, D.W. (1964). Effect of ischemia on known substrates + cofactors of glycolytic pathway in brain. J. Biol. Chem. *239*, 18–30.

Mandal, R., Guo, A.C., Chaudhary, K.K., Liu, P., Yallou, F.S., Dong, E., Aziat, F., and Wishart, D.S. (2012). Multi-platform characterization of the human cerebrospinal fluid metabolome: a comprehensive and quantitative update. Genome Med. *4*, 38.

McDermott, S.P., Eppert, K., Lechman, E.R., Doedens, M., and Dick, J.E. (2010). Comparison of human cord blood engraftment between immunocompromised mouse strains. Blood *116*, 193–200.

Minati, L., Aquino, D., Bruzzone, M.G., and Erbetta, A. (2010). Quantitation of normal metabolite concentrations in six brain regions by in-vivoH-MR spectroscopy. J. Med. Phys. *35*, 154–163.

Murphy, R.C., Hankin, J.A., and Barkley, R.M. (2009). Imaging of lipid species by MALDI mass spectrometry. J. Lipid Res. *50* (*Suppl*), S317–S322.

Nicholson, J.K., Holmes, E., Kinross, J.M., Darzi, A.W., Takats, Z., and Lindon, J.C. (2012). Metabolic phenotyping in clinical and surgical environments. Nature *491*, 384–392.

Nikolskiy, I., Mahieu, N.G., Chen, Y.J., Tautenhahn, R., and Patti, G.J. (2013). An untargeted metabolomic workflow to improve structural characterization of metabolites. Anal. Chem. *85*, 7713–7719.

O'Callaghan, J.P., and Sriram, K. (2004). Focused microwave irradiation of the brain preserves in vivo protein phosphorylation: comparison with other methods of sacrifice and analysis of multiple phosphoproteins. J. Neurosci. Methods *135*, 159–168.

Patti, G.J., Shriver, L.P., Wassif, C.A., Woo, H.K., Uritboonthai, W., Apon, J., Manchester, M., Porter, F.D., and Siuzdak, G. (2010). Nanostructure-initiator mass spectrometry (NIMS) imaging of brain cholesterol metabolites in Smith-Lemli-Opitz syndrome. Neuroscience *170*, 858–864.

Patti, G.J., Tautenhahn, R., and Siuzdak, G. (2012a). Meta-analysis of untargeted metabolomic data from multiple profiling experiments. Nat. Protoc. *7*, 508–516.

Patti, G.J., Yanes, O., Shriver, L.P., Courade, J.-P., Tautenhahn, R., Manchester, M., and Siuzdak, G. (2012b). Metabolomics implicates altered sphingolipids in chronic pain of neuropathic origin. Nat. Chem. Biol. *8*, 232–234.

Patti, G.J., Yanes, O., and Siuzdak, G. (2012c). Innovation: metabolomics: the apogee of the omics trilogy. Nat. Rev. Mol. Cell Biol. *13*, 263–269.

Pears, M.R., Cooper, J.D., Mitchison, H.M., Mortishire-Smith, R.J., Pearce, D.A., and Griffin, J.L. (2005). High resolution 1H NMR-based metabolomics indicates a neurotransmitter cycling deficit in cerebral tissue from a mouse model of Batten disease. J. Biol. Chem. *280*, 42508–42514.

Piomelli, D., Astarita, G., and Rapaka, R. (2007). A neuroscientist's guide to lipidomics. Nat. Rev. Neurosci. *8*, 743–754.

Pouwels, P.J.W., and Frahm, J. (1998). Regional metabolite concentrations in human brain as determined by quantitative localized proton MRS. Magn. Reson. Med. *39*, 53–60.

Prabakaran, S., Swatton, J.E., Ryan, M.M., Huffaker, S.J., Huang, J.T., Griffin, J.L., Wayland, M., Freeman, T., Dudbridge, F., Lilley, K.S., et al. (2004). Mitochondrial dysfunction in schizophrenia: evidence for compromised brain metabolism and oxidative stress. Mol. Psychiatry *9*, 684–697, 643.

Rae, C. (2014). Metabolomics in neuroscience and disease. In Global Metabolic Profiling: Clinical Applications (London: Future Science), pp. 162–180.

Rongvaux, A., Willinger, T., Martinek, J., Strowig, T., Gearty, S.V., Teichmann, L.L., Saito, Y., Marches, F., Halene, S., Palucka, A.K., et al. (2014). Development and function of human innate immune cells in a humanized mouse model. Nat. Biotechnol. *32*, 364–372.

Salem, N., Jr., Litman, B., Kim, H.Y., and Gawrisch, K. (2001). Mechanisms of action of docosahexaenoic acid in the nervous system. Lipids *36*, 945–959.

Sjövall, P., Lausmaa, J., and Johansson, B. (2004). Mass spectrometric imaging of lipids in brain tissue. Anal. Chem. *76*, 4271–4278.

Smith, C.A., Want, E.J., O'Maille, G., Abagyan, R., and Siuzdak, G. (2006). XCMS: processing mass spectrometry data for metabolite profiling using nonlinear peak alignment, matching, and identification. Anal. Chem. *78*, 779–787.

Sporns, O. (2011). The human connectome: a complex network. Ann. N Y Acad. Sci. *1224*, 109–125.

Strott, C.A., and Higashi, Y. (2003). Cholesterol sulfate in human physiology: what's it all about? J. Lipid Res. *44*, 1268–1278.

Tautenhahn, R., Patti, G.J., Rinehart, D., and Siuzdak, G. (2012). XCMS Online: a web-based platform to process untargeted metabolomic data. Anal. Chem. *84*, 5035–5039.

Tkác, I., Henry, P.G., Andersen, P., Keene, C.D., Low, W.C., and Gruetter, R. (2004). Highly resolved in vivo 1H NMR spectroscopy of the mouse brain at 9.4 T. Magn. Reson. Med. *52*, 478–484.

Umhau, J.C., Zhou, W., Carson, R.E., Rapoport, S.I., Polozova, A., Demar, J., Hussein, N., Bhattacharjee, A.K., Ma, K., Esposito, G., et al. (2009). Imaging incorporation of circulating docosahexaenoic acid into the human brain using positron emission tomography. J. Lipid Res. *50*, 1259–1268.

Vaishnavi, S.N., Vlassenko, A.G., Rundle, M.M., Snyder, A.Z., Mintun, M.A., and Raichle, M.E. (2010). Regional aerobic glycolysis in the human brain. Proc. Natl. Acad. Sci. USA *107*, 17757–17762.

Vance, J.E. (2012). Dysregulation of cholesterol balance in the brain: contribution to neurodegenerative diseases. Dis. Model. Mech. *5*, 746–755.

Wei, J., Buriak, J.M., and Siuzdak, G. (1999). Desorption-ionization mass spectrometry on porous silicon. Nature *399*, 243–246.

Yanes, O., Tautenhahn, R., Patti, G.J., and Siuzdak, G. (2011). Expanding coverage of the metabolome for global metabolite profiling. Anal. Chem. *83*, 2152–2161.

